Upwelling Analysis Of Moroccan Atlantic Coast Based On Satellite Data.

Zahra Okba[1*], Othman Cherkaoui Dekkaki[2], Hassan Elouizgani[1]

[1*]Laboratory of Aquatic systems, Marine, and Continental environment, Faculty of Sciences, Agadir, Morocco.
[2]LAMA Laboratory, Faculty of Sciences, University Mohammed V in Rabat, Morocco.

***Corresponding Author:** Zahra Okba
*Laboratory of Aquatic systems, Marine, and Continental environment, Faculty of Sciences, Agadir, Morocco,
zahra.okba@edu.uiz.ac.ma

Abstract:
Spatio-temporal upwelling patterns were studied along the Moroccan Atlantic Coast 11 for 2015–2020 to scale upwelling intensity using chlorophyll-a (Chl-a) concentration as a reference upwelling proxy for relative biomass increase. Morocco's south coast has been under permanent upwelling regimes characterized by lower coastal sea surface temperatures (SSTs) han oceans of the same latitude. This regime is consistent with wind-derived Ekman transport, (UIE). The index shows year-round upwelling-favorable conditions in the south. However, it has, an annual cycle characterized by more favorable conditions in April-August, peaking in July, and, less upwelling-favorable conditions in October-March, with a minimum in February. Compared to, the north, a high chlorophyll concentration has been observed in the south of the Moroccan coast.

Keywords: Upwelling Index, Canary Upwelling system, Moroccan coast, Chlorophyll, SST, Wind force, Fisheries.

1Introduction

Morocco is located in the Canary Upwelling System (CanUS) and is one of the four main Eastern Boundary Upwelling Systems (EBUS) known to have a major impact on the primary productivity of the respective ecosystem and thus on the abundance, diversity, distribution, and production of marine organisms. At all trophic levels, coastal areas along the western boundaries of the continents are characterized by trade winds that induce Ekman transport from the coast. This leads to increased cold, nutrient-rich water in the coastal zone, which contributes to intense biological activity near the coast (Chavez and Messie´, 2009). Alternating strong/released trade winds lead to a succession of active/inactive upwelling events reflected by changes in sea surface temperatures (SST) and chlorophyll production. Furthermore, pelagic ecosystems and the Atlantic coast of Morocco are governed by spatial and temporal variations in upwelling activity. The upwelling maintains high biological productivity and therefore a high fisheries production, mainly in the southern area where fishing activity is very important. Moreover, this ecosystem is subject to Spatiotemporal variability at different scales, which plays an important role in life cycles (Benazzouz et al., 2014). Upwelling has been studied for decades using various statistical models and simulations. (Bakun, 1989; Bakun et al., 2010; Bonino et al., 2019; Wang et al., 2015). However, most upwelling trend studies use sampled and monthly averaged wind and temperature variables. Here, we sought to analyze upwelling characteristics across the western and northern coast of Morocco over the past half-decade (2015 to 2020). The analysis was performed in terms of upwelling indices calculated from Ekman transport data (UIE), to detect upwelling fluctuations and changes over time. The biological phenology of many marine ecosystem processes is strongly influenced by and dependent on upwelling events such as duration, frequency, and intensity. (Barth et al., 2007). Upwelling events can cause significant or minimal disturbance, depending on their characteristics. (Benoit-Bird et al., 2019). The ecosystem implications of upwelling events have been characterized by sea surface temperature and chlorophyll concentrations. Thus, wind-induced upwelling conditions and the response of the water to this forcing will be analyzed simultaneously along the coast. However, upwelling also affects other marine communities, and changes in upwelling patterns can have dramatic effects on them. (Wang et al., 2015). This paper aims to show how Ekman transport-based upwelling indices calculated from satellite data relate to Sea surface temperature, chlorophyll a, wind, and fisheries data in time and space, to compare the tendencies of the upwelling indices to previous studies, to investigate and document interannual variabilities of Moroccan coastal upwelling, and to identify fluctuations during the period of investigation. The period (2015-2020) chosen covers an important event that affects ocean health, the 2016 is the warmest year on record globally due to climate change, and from December 2019 there was one of the largest pandemics outbreaks of all times (covid-19).

2 MATERIALS AND METHODS

In this section, we describe the observation data used, and the definition of the upwelling indices (UI)

2.1 Area of study

The study area consists of nine Moroccan coastal cities spread over eight coastal regions from the 62 northern (Tanger) to the southern (Dakhla).

2.2 Sea Surface Temperature Dataset

SST is considered a preeminent variable in the ocean-atmosphere coupling system and is a handy research tool in the scientific fields of meteorology and oceanography. SST data have been collected using field measurement technologies for more than 150 years, and SST satellite measurements have been available since the late 1970s. Over the past decade, technologies have been

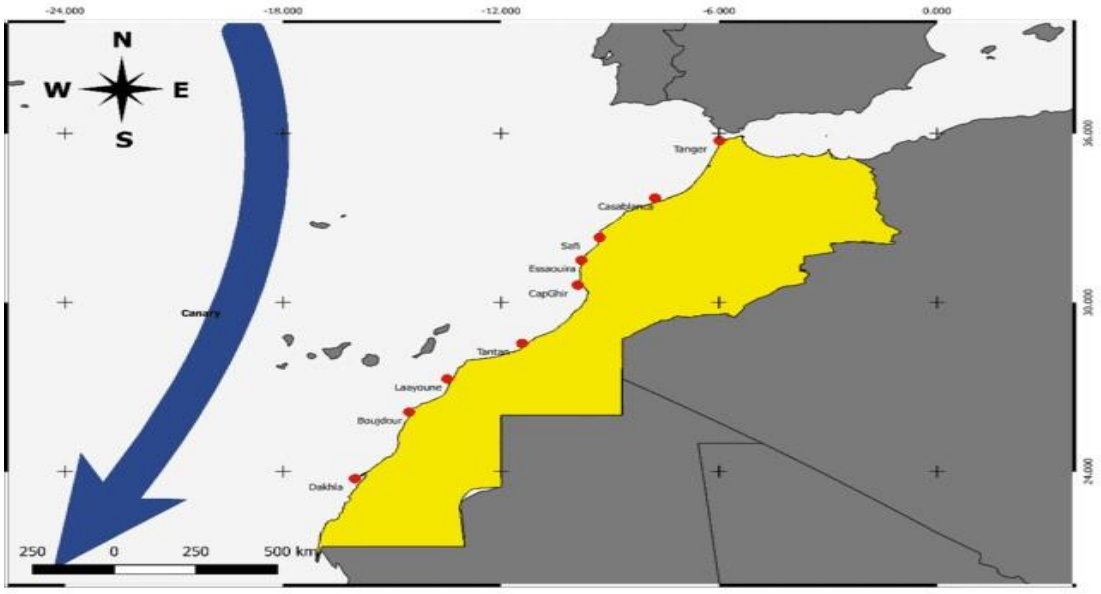

Figure 1: Geography of the Moroccan coast (the red dots represent the geographical locations of the study area)

developed to assimilate and blend different SST data sets from different fields and satellite platforms. These are referred to as Level 3 and Level 4 products, and Level 4 data are transparent and widely used in coastal studies.

The assessment of variability in the upwelling dynamics is dealt with in this paper, where we made a grid from optimally interpolated sea surface temperatures (dOISST, *v*.2.1) daily 0.25 from the National Oceanic and Atmospheric Administration (NOAA) worldwide. In this remote sensing satellite product, gaps in spatial coverage are filled by interpolating data collected from ships and buoys (Banzon et al., 2016; Reynolds et al., 2007). The dOISST data product was collected on the ERDDAP server using the rerddap package in R (Abrahams et al., 2021) for nearly the last halfdecade, providing us with a long time series (6 years).

2.3 Satellite Wind Dataset

Wind speed and direction were determined using the rWind library (Ferna´ndez-Lo´pez & Schliep, 2019) in R for statistical calculations and graphing. This library is specifically designed to download and process wind and current data from the global forecasting system. rWind provides a simple workflow from data download to cost analysis across sites. The rWind library bridges the gap between the accessibility of ocean wind and current data and its incorporation into general frameworks applicable to ecological or evolutionary research. From these data, we obtained the speed and direction of ocean winds/currents.

2.4 Chlorophyll

A time series of monthly satellite chlorophyll data products for the period 2015-2020 from MODISAqua were obtained from the ERDDAP Web portal, for the region of Morocco ($(-20)-(-5)W$ and $36-89\ 20N$) using the rxtracto 3D function. Chlorophyll a is commonly used as a proxy for phytoplankton biomass.

2.5 Fisheries Production

To assess the usefulness of ET-UI and to explain fisheries production, the statistics were used taken from the Ministry of Agriculture, Maritime Fisheries, Rural Development and Water and Forests Department of Maritime Fisheries database (Ministe`re de l'Agriculture, 2020). We obtained the 95 amount of coastal and artisanal fishing catches per region between 2015 and 2020.

2.6 Upwelling identification

There are different approaches to estimating the occurrence of upwelling, including coastal temper- ature and wind variables and a range of Ekman processes. The Ekman transport upwelling index is appropriate if the primary forcing of the upwelling mechanism is mainly caused by wind stress

[0]https://upwell.pfeg.noaa.gov/erddap/griddap/erdMBchla1day.html

along the coast (Naulita et al., 2020), which is the case on the Moroccan coast. To calculate the Ekman transports in each cross-shore direction, the coordinate system was rotated in each region according to:

$$UI = -(\sin(\theta - \pi/2)Q_x + \cos(\theta - \pi/2)Q_y).$$

Where Q_x and Q_y are the zonal and meridional components of the Ekman transport, respectively, and θ is the average angle between the coastline and the equator. θ = 55 degrees were taken as the average coastal angle in our study. Using this definition, positive (negative) upwelling indices correspond to favorable (unfavorable) upwelling conditions. (Bakun, 1973) defined by the upwelling index (UI), which is positive (negative) when the transport is offshore (onshore). The previous equation produces a value called the upwelling index. This upwelling index is based on wind speed and direction to identify favorable conditions for upwelling. Since upwelling is affected by wind patterns, (Bakun, 1989) predicted that variability in wind patterns would affect the intensity of the upwelling signal. As a starting point, we provided SST satellite imagery to understand how the temperatures of these cold waters change over time. ERD has been publishing the Bakun upwelling index every 6 hours at 15 designated locations for many years. To calculate the upwelling index, we use the xtractomatic(Mendelssohn, 2018) package on R. 'Upwell' was defined as a function that rotates the Ekman transport value to obtain the offshore component (upwelling index) and also defines a plotUpwell function that plots the upwelling. xtracto 3D can download the Ekman transports calculated from the Fleet Numerical Meteorological and Oceanographic Center (FNMOC) pressure field.

3 Results and Discussion

In this paper, we analyzed the Spatio-temporal evolution of the upwelling pattern on the Moroccan coast. Three different data, SST, chlorophyll, and Upwelling index Ekman transport-based data from 2015 to 2020, have been used to better describe the main features of one of the major 117 upwelling regions of the world.

3.1 The dynamics of upwelling as shown by the Ekman Upwelling Index

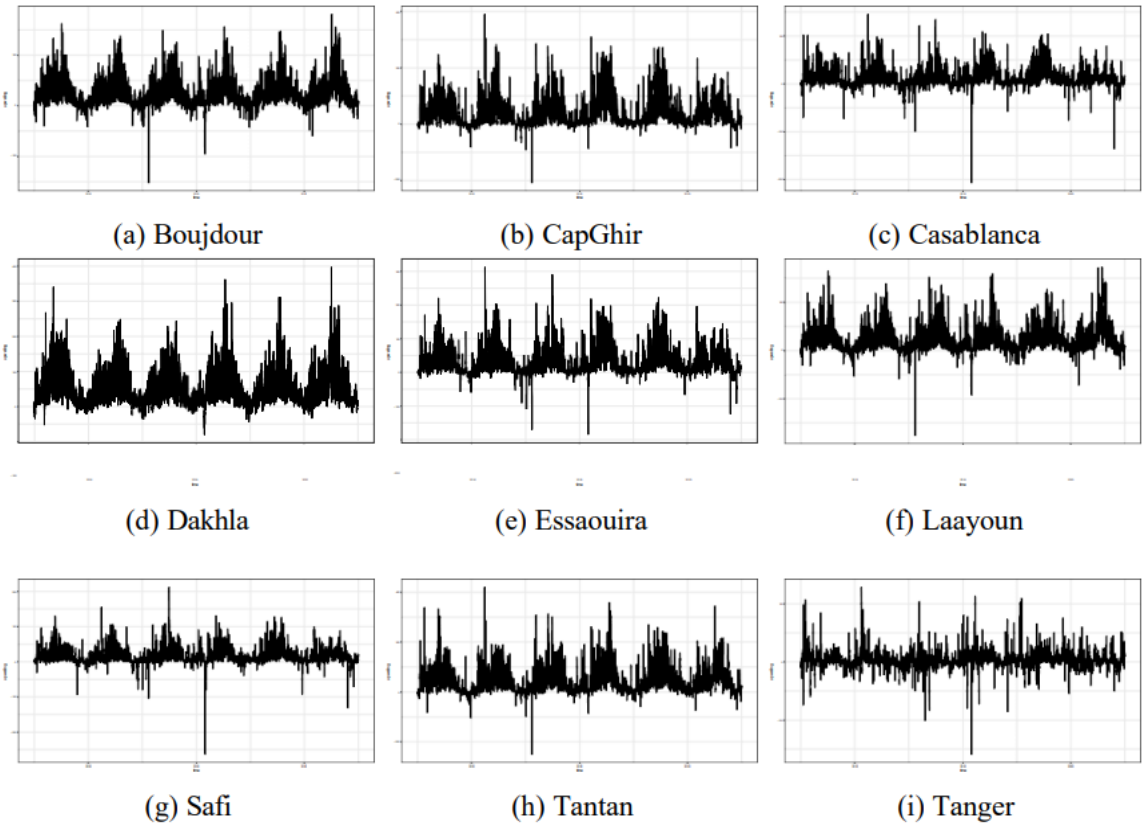

Figure 2: Annual cycle of the upwelling index UIE, calculated from Ekman transport during the period 2015-2020

It is common to employ ET-UI to identify upwelling areas, as shown in Figure 2. Generally, pos itive (negative) UIE values mean upwelling favorable (unfavorable) conditions. The higher the UI value, the more intense upwelling occurs (Naulita et al., 2020). The graph corresponds to the appearance of each month on the major and minor upwelling-favorable partitions. It shows the prevalence of more favorable conditions for upwelling from April to September and less favorable conditions for upwelling from October to March during the period 2015– 2020. The seasonal pattern corresponding to autumn-winter (October–March) is characterized by an Ekman transport perpendicular to the shore, being the maximum intensity on the order of $150 m^3 s^{-1} km^{-1}$ at the southernmost part (from CapGhir to Dakhla). In addition, the upwelling intensity is observed to increase southward. The pattern corresponding to spring-summer (April–September) is considerably different. In particular, the most intense upwelling events are observed from April to September, peaking

from July to August. The maximum transport intensities are on the order of $400m^3s^{-1}km^{-1}$ in the southernmost part of Morocco. Maximum values are obtained at all points from April to August, and minimum values from October to February. In addition, the upwelling intensity is observed to increase southward. The index shows some negative values representing a "downwelling" or absence of upwelling activity in winter that can reach $(-260m^3s^{-1}km^{-1})$. Upwelling activity is relatively weak in winter and increases gradually in spring to reach maximum activity during the summer seasons. It begins gradually to decrease in the fall seasons. In February 2017/2018, for each site, we can observe that it presents negative indices suggesting downwelling.

The upwelling maximum ("upwelling favorable") is centered around Capghir in summer and all the years south of TanTan. Minima occur in the north (Tanger, Casablanca, Safi) in the winter with a negative value ("downwelling favorable"). This activity increases gradually in winter (between 50 and $160m^3s^{-1}km^{-1}$) and reaches its maximum peak in summer during July $(500m^3s^{-1}km^{-1})$.

It gradually decreases in autumn (between 60 and $150m^3s^{-1}km^{-1}$). The evolution of UIE (Figure 2) shows that the periods characterized by conditions more favorable to upwelling correspond to April-August with higher values (as large as $400m^3s^{-1}km^{-1}$) on the coastline in May/June and July, respectively. The fluctuation of wind force directly affects the ocean water and the ecosystem in Northern Morocco. In contrast, the southern regions are characterized by cold, upwelled water (Figure 2), even in the months with low values of UIE. In the southern, the inter-annual evolution of UIE and SST are in phase (higher values of UIE correspond to lower SST) (Figure 2 and Figures 3,4,5,6), which means that the upwelling is tightly linked to the seasonality of the trade winds, 150 without time lag, in agreement with the results of (Benazzouz et al., 2014) in the same area.

3.2 Sea Surface Temperature Analysis using satellite imagery

To support these ET-UI results, we analyzed satellite-derived SST data, considering relatively cold water origins from below that are pumped up by coastal upwelling. The seasons with the most and least upwelling favorable conditions are respectively spring-summer and autumn-winter. In February(winter) and November(autumn), the cold upwelled water can be detected only on the southern Moroccan coast with a weak difference in temperature. However, in May (spring), the cold upwelled water is evident in southern Morocco and much colder in 2018, with temperatures from $16 - 17C$. We can see that during August(summer), the upwelled water is shown all over the Moroccan coast. In southern Morocco, the upwelled water gets colder gradually, contrary to northern Morocco, where it gets warmer. The time series of the monthly UIE (Figure 2) and SST (Figures 3,4,5,6) summarizes the main inter-annual characteristics of the upwelling seasons in the period 2015-2020. The Ekman transport is more substantial in 2018 compared to the following years (Figure 2) and leads to a colder SST than $17C$ in southern Morocco (Figures 3,4,5,6). Fluctuations of UIE where the maximum Ekman transport appears between July and August. The upwelling favorable Ekman transport is generally more intense in the south of Morocco, where it is in phase with the occurrence of the SST minimal values (Figures 3,4,5,6).

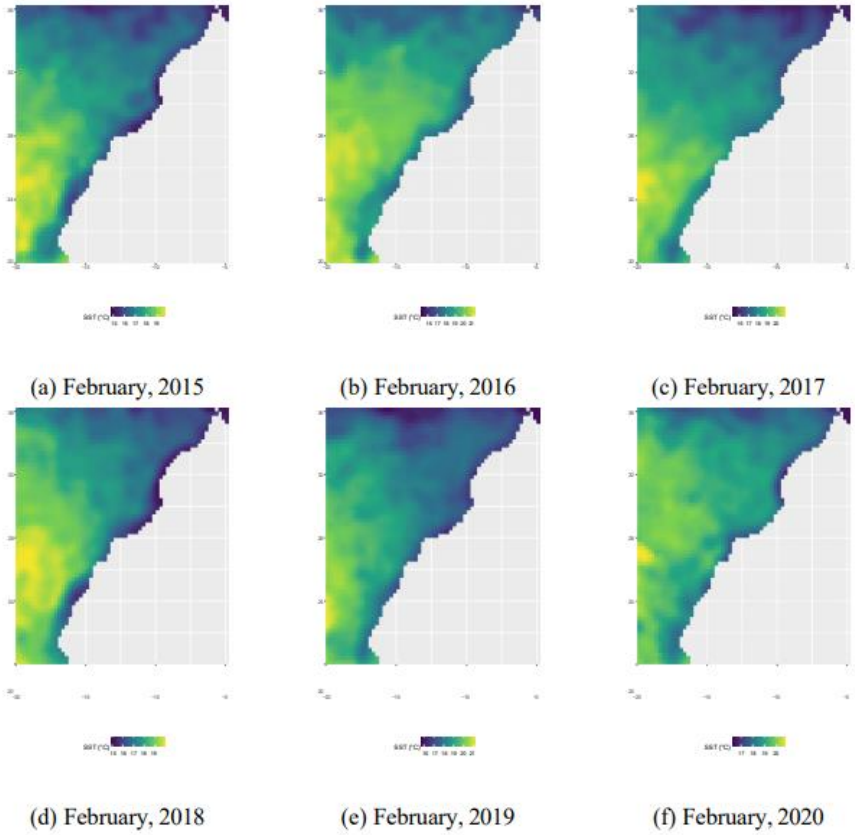

Figure 3: Month of February SST imageries along the Moroccan coast for 2015-2020

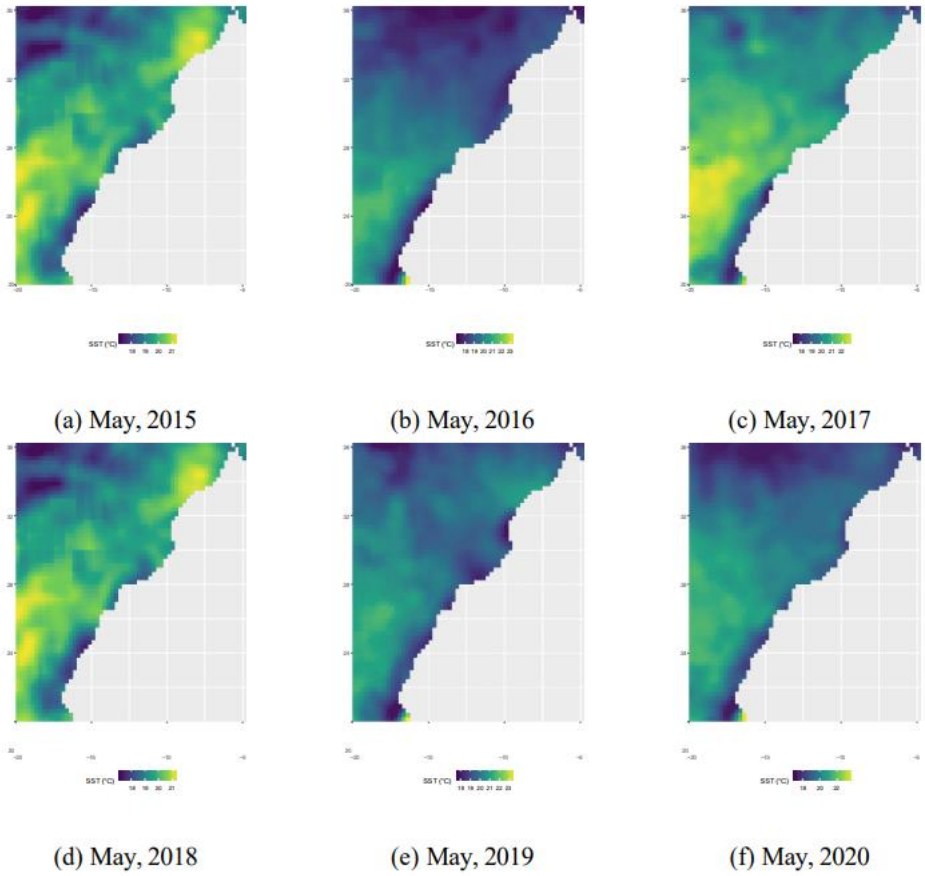

(a) May, 2015 (b) May, 2016 (c) May, 2017

(d) May, 2018 (e) May, 2019 (f) May, 2020

Figure 4: Month of May SST imageries along the Moroccan coast for 2015-2020

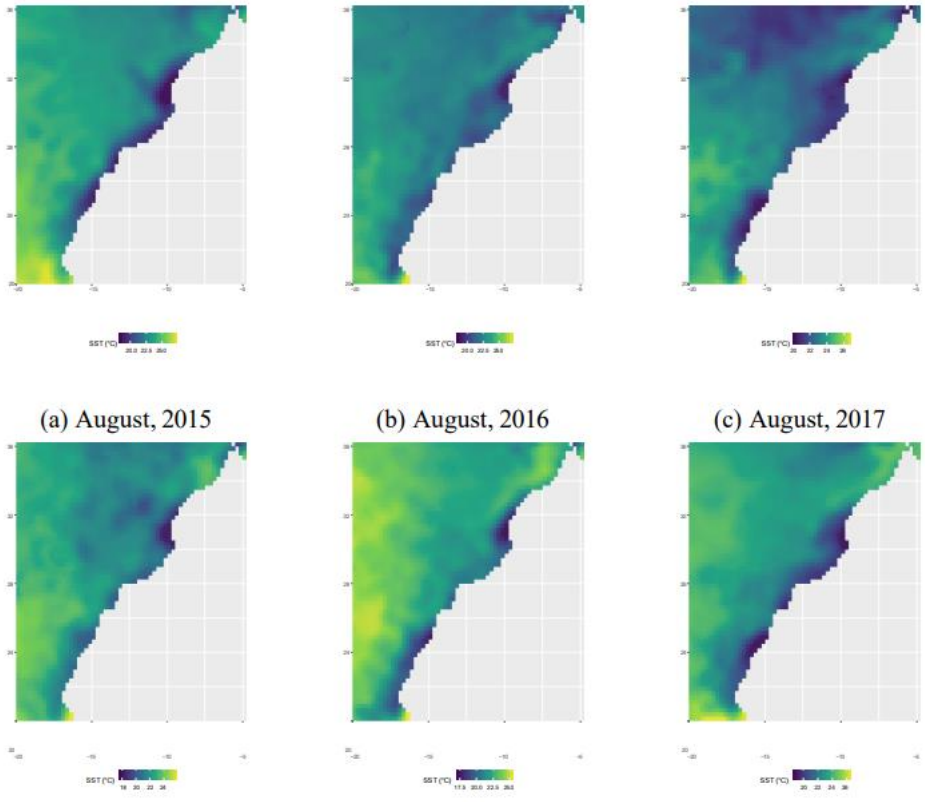

(a) August, 2015 (b) August, 2016 (c) August, 2017

(d) August, 2018 (e) August, 2019 (f) August, 2020

Figure 5: Month of August SST imageries along the Moroccan coast for 2015-2020

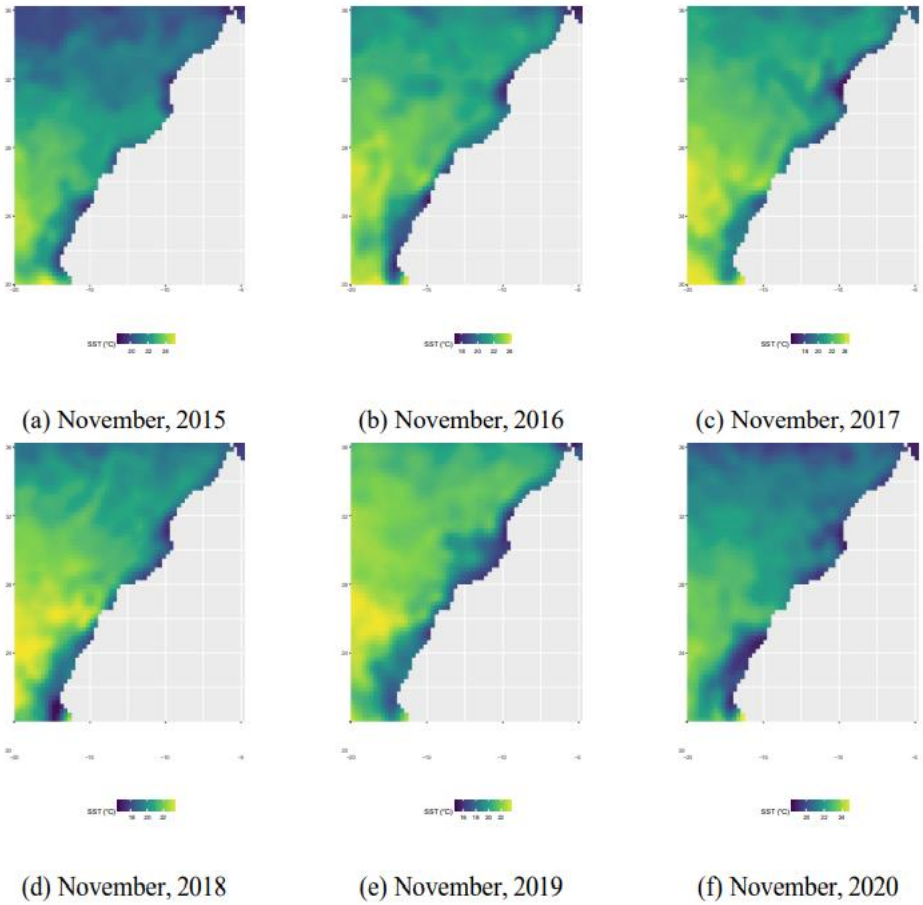

Figure 6: Month of November SST imageries along the Moroccan coast for 2015-2020

3.3 Wind Forcing

Figures 7,8,9,10 shows that the wind direction parallels the Moroccan coastline in summer, contrary to winter. In February 7 and November 10, the wind direction is irregular on most Moroccan coasts, with wind speeds varying between $0ms^{-1}$ and $0ms^{-1}$. For May 8 and August 9, the wind direction is parallel to the coast in the southern areas. It is irregular in northern areas, particularly from 2015 to 2017, and in central Morocco (CapGhir) between 2017 and 2020. At that time of the year, the wind speed varies from $4ms^{-1}$ to $8ms^{-1}$. According to(Li et al., 2019), upwelling favorable wind events are defined to have a wind speed greater than $5ms^{-1}$. In some studies, considering the wind speed threshold of $5ms^{-1}$, the minimum speed of wind events required to bring cold water to the surface (Largier et al., 2006; Wilkerson et al., 2006) has been defined.

Where permanent upwelling exists, trade winds of $20 - 25N$ occur throughout the year. The winter trade winds that continue south of 20N will ease in the summer. And the sustained summer trade winds north of $25N$ ease in winter. North of $26N$, they describe the weak permanent annual upwelling zone mentioned above. In this zone, the highest upwelling intensity is recorded during the summer months but occurs throughout the year. Northern Morocco shows the weakest upwelling (intensity between $2ms^{-1}$ and $5ms^{-1}$), mainly due to weak winds and an unfavorable coastline orientation. Upwelling is significantly more vigorous in central Morocco (up to $8ms^{-1}$ in summer near Cape Ghir) Figure 9. The Southern Morocco region ($21–26N$) is characterized by solid and quasi-permanent upwelling and trade winds, with only two relative minimums in March and 186 August, due to the residual influence of the seasonal minimum of the trade winds in winter in the northern part (Tanger, Casablanca, Safi, Essaouira) of the system and summer in its southern part 1 (Capghir, Tantan. Laayoune, Boujdour, Dakhla). The Southern Morocco region is characterized by a constantly high upwelling activity, with the maximum wind in summer and more relaxation during winter. In this sense, (Marrero-Betancort et al., 2020) confirmed that in this region (the Moroccan Coast), the most intense winds occur during summer and spring, as expected. The lowest intensity was found during autumn and winter.

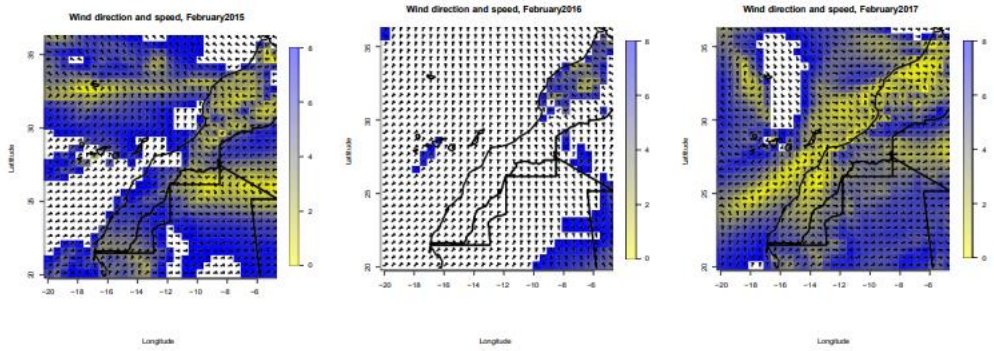

(a) February, 2015 (b) February, 2016 (c) February, 2017

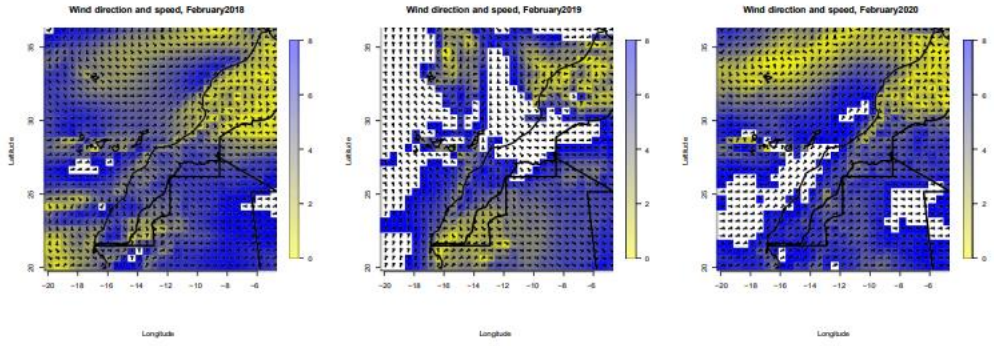

(d) February, 2018 (e) February, 2019 (f) February, 2020

Figure 7: Wind direction and speed for the moth of February for the period 2015-2020.

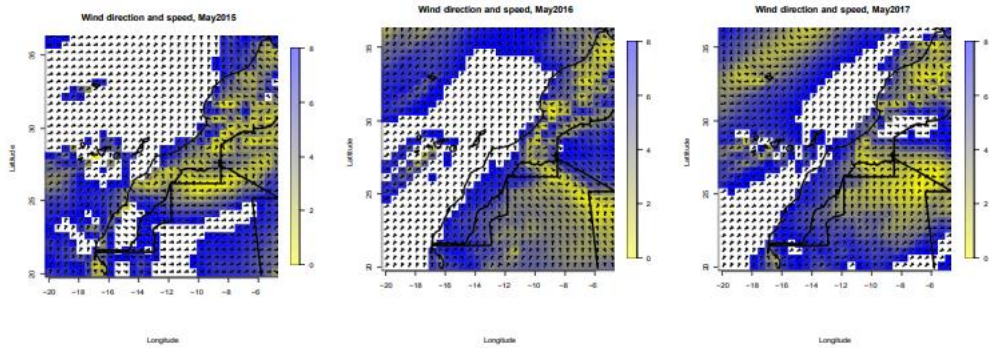

(a) May, 2015 (b) May, 2016 (c) May, 2017

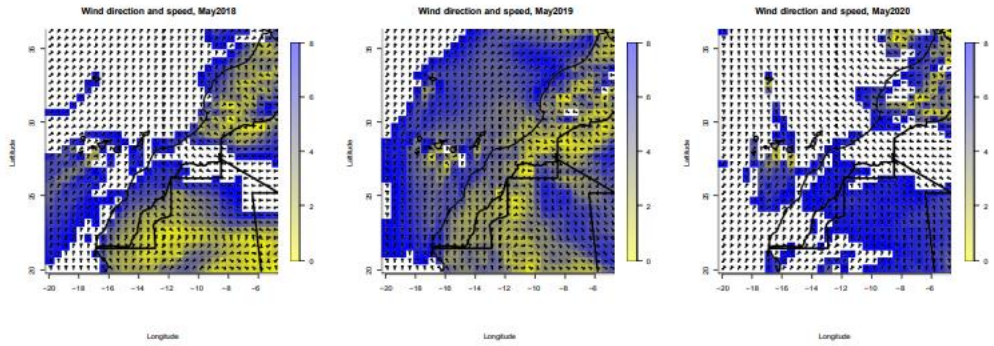

(d) May, 2018 (e) May, 2019 (f) May, 2020

Figure 8: Wind direction and speed for the moth of May for the period 2015-2020.

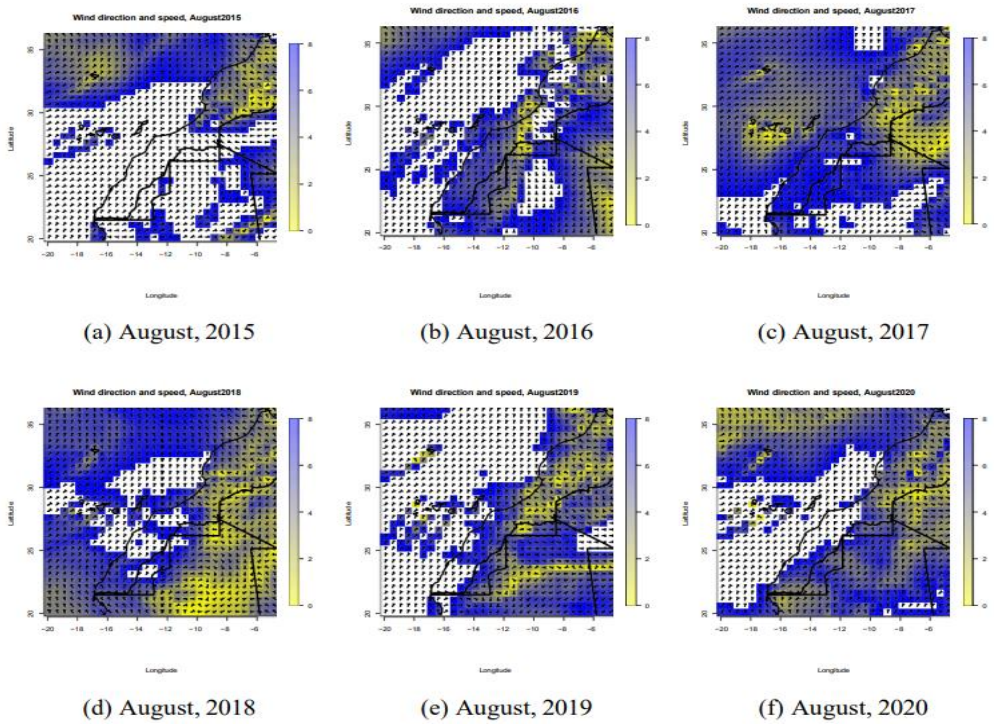

(a) August, 2015 (b) August, 2016 (c) August, 2017

(d) August, 2018 (e) August, 2019 (f) August, 2020

Figure 9: Wind direction and speed for the moth of August for the period 2015-2020.

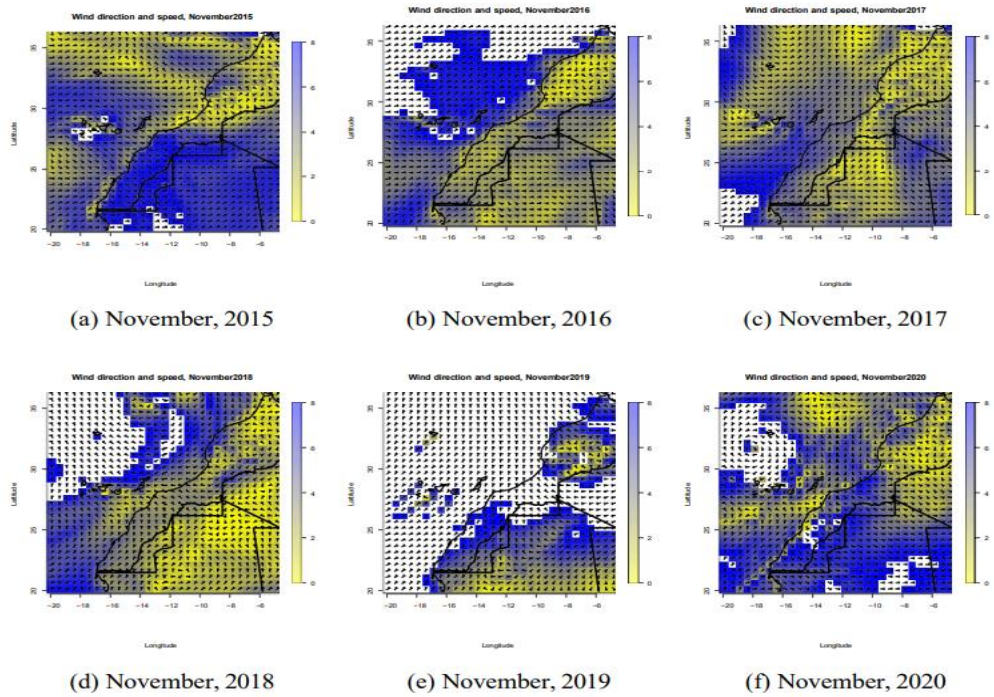

(a) November, 2015 (b) November, 2016 (c) November, 2017

(d) November, 2018 (e) November, 2019 (f) November, 2020

Figure 10: Wind direction and speed for the moth of November for the period 2015-2020.

3.4 Chlorophyll Variability and Fisheries Statistics

We used the chlorophyll-a (Chl-a) concentration as a proxy for phytoplankton biomass and production to study the biological response to upwelling. The upwelling intensity often leads to a high chlorophyll-a level because the upwelled water mass is nutrient-rich water, which triggers a high phytoplankton growth (Naulita et al., 2020).

Firstly, southern Morocco exhibits the typical increase of Chla during the months of upwelling (values generally more significant than $5mg.m^3$ between April and August) and more accentuated 200 increases in the southern regions during the upwelling seasons of 2016, 2017, and 2018; and in the Northern regions during 2018 and 2019. In the south, maximum values of Chl-a are observed in summer (August-September) and early fall (October-November) that reach $45mg.m^3$. In the northern regions, the maximum values occurred in the fall of 2018 - 2019 ($17mg.m^3$) and in the winter of 2015 and 2016 ($5mg.m^3$). Satellite observation of Sea Surface Temperature (SST) and Chlorophyll-a concentration can be used to identify upwelling regions of Morocco. From the map (Figure 11), cold waters near the coast combined with high Chlorophyll concentrations indicate 207coastal upwelling events. A better understanding of Morocco's upwelling

variability is essential 208 to properly managing and protecting these ecologically and economically important coastal areas.

The coastal upwelling of Morocco can also affect productivity across the Atlantic Ocean. The response of high primary production to upwelling lags behind the physical process of wind-driven upwelling, and the peak phytoplankton population available to secondary consumers is even lagging behind the physical upwelling process. During the upwelling, the seed stock of phytoplankton cells in deep nutrient-rich water on the shelf is lifted into the well-lit, shallow water. The freshly upwelled water is characterized by low chlorophyll concentration, high nutrients, low temperature, and low minimal processes. When the water is carried to the euphotic zone, phytoplankton responds to intense light and nutrients, turning on nutrient uptake mechanisms and initiating photosynthesis, as confirmed by (Largier et al., 2006), which explains the delay in chlorophyll production in fall and winter contrary to the upwelling phenomena that is highest during summer and starting in spring. The aging upwelled water is characterized by high chlorophyll, low or rapidly decreasing nutrients, rising water temperature, and high/ maximal phytoplankton rate processes.

The graph (Figure 12) shows that southern fisheries production is more significant, with the maximum occurring at Dakhla Laayoune and Tantan. The quantity captured in the north of Morocco is lower than the minimum in Essaouira. The weak chlorophyll productivity can explain this, in the north (maximum is $17 mg.m^3$) compared to the high productivity in the south, which can reach $45 mg.m^3$. The implications of upwelling for the ecosystem have been characterized using the time series of the Chl-a concentrations (Figure 11). In the south of Morocco, Chl-a shows a high variability related to the occurrence of upwelling and non-upwelling seasons; the highest concentration values are observed in Tantan during the upwelling seasons of 2017 and in Laayoune in 2016. In the northern regions, the Chla shows lower values (Figure 11). The SST maps (Figures 3,4,5,6) allow the Coldwater filaments' discrimination associated with upwelling events along the Moroccan coast. These recurrent upwelling filaments (SST lower than $18C$) are generally located in southern Morocco. Upwelling conditions were analyzed in terms of Ekman transport upwelling index and SST, time series of the satellite Chla, and wind products. Chlorophyll-a concentration in the south of Morocco is persistently greater and more permanent when compared with the north of Morocco. It becomes evident that upwelling in the southern waters of the Moroccan coast is stable with solid intensity.

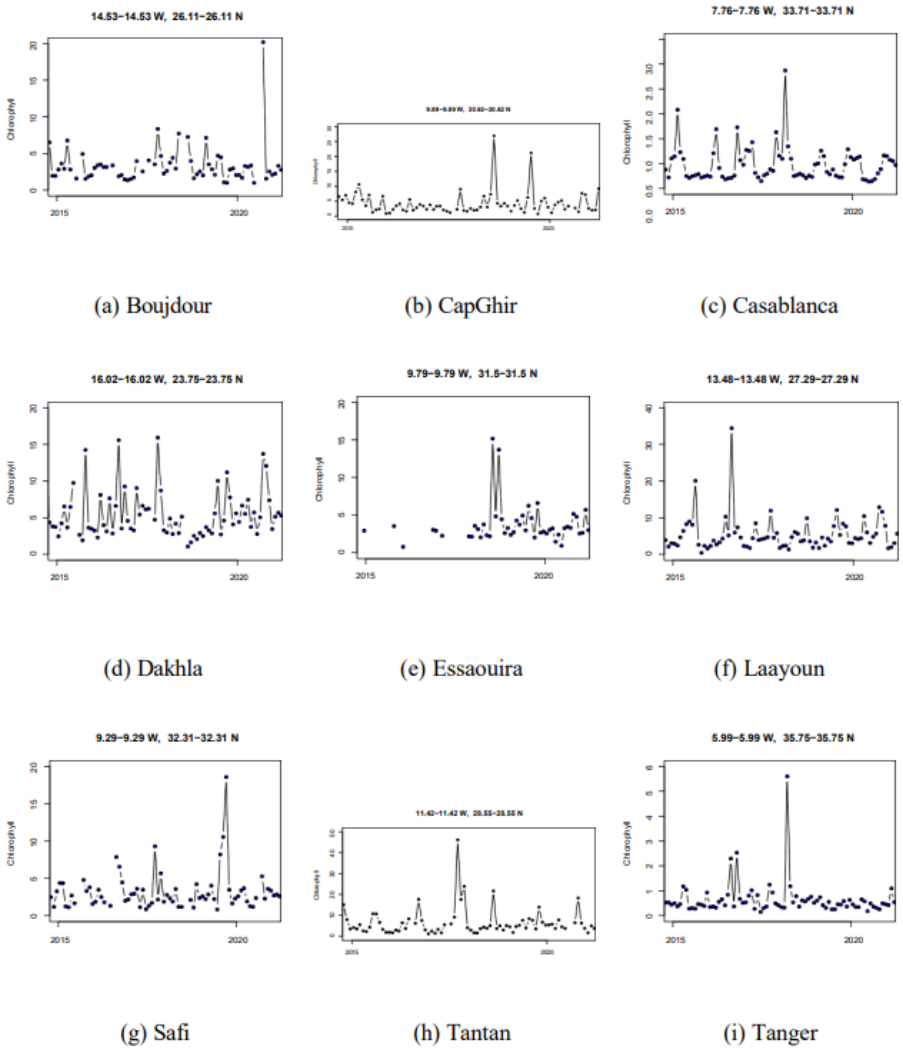

Figure 11: Chlorophyll-a concentration (mgm^3) time series for the period 2015-2020

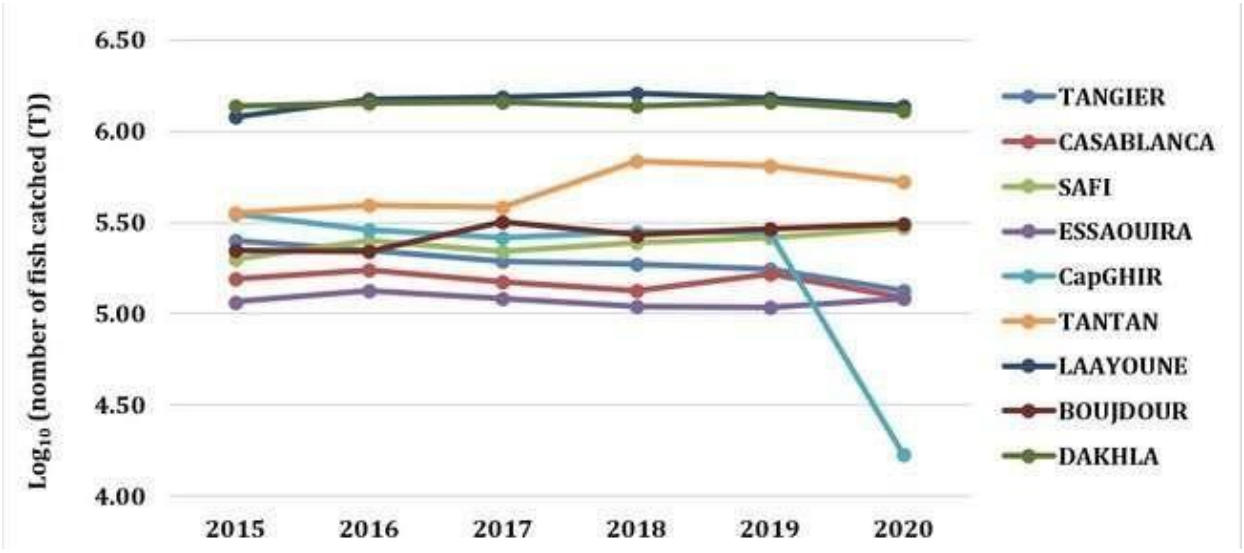

Figure 12: Evolution of coastal and artisanal fishing catches by region from 2015 to 2020 In weight (in Log_{10}(tonnes))

4 Conclusion

In this work, we focused on deeply understanding the interplay of the upwelling and its responses to the wind force since phenomena in this region are driven mainly by wind force. We analyzed the Upwelling phenomena along the Moroccan Atlantic coast using the Ekman transport-based upwelling index, wind data, Sea Surface Temperature, and Chlorophyll data between 2015 and 2020. These results show the sustainability of high biomass coastal waters in this strong advection and wind-dominated system. We found that in southern Morocco, more intense upwelling occurs (mainly in spring-summer) than in the north, which is caused by wind direction and speed. The South is under a permanent upwelling regime which is in good agreement with previous studies; the upwelling index (UIE) follows an annual cycle with maximum intensity in July and a minimum in February. We observed that primary production in the South is significant, mainly in the fall winter ($45mg.m^3$) when compared with the north ($5mg.m^3$), which affects fisheries production.

Availability of data and material

The authors declare that all data supporting the findings of this study are available within the article 251 (For details about the material used are mentioned in section 2).

Conflict of Interest

The authors declared that they have no conflict of interest.

References

1. [Abrahams et al., 2021] Abrahams, A., Schlegel, R.W., Smit, A.J., [2021]. *Variation and Change* 256 *of Upwelling Dynamics Detected in the World's Eastern Boundary Upwelling Systems*. Front. Mar. Sci. 8, 1–11.https://doi.org/10.3389/fmars.2021.626411.
2. [Bakun, 1989] Bakun, A., 1989. *L'oce´an et la variabilite´ des populations marines*. In : Troadec J.P. (Eds.), L'homme et les ressources halieutiques : Essai sur l'usage d'une ressource renouvelable. IFREMER, Brest, 155-188.
3. [Bakun, 1973] Bakun, A., 1973. *Coastal Upwelling Indices*, West Coast of North America, 1946- 71.
4. [Bakun et al., 2010] Bakun, A., Field, D.B., Redondo-Rodriguez, A., Weeks, S.J., 2010. *Green-* 264 *house gas, upwelling-favorable winds, and the future of coastal ocean upwelling ecosystems*. Glob. Chang. Biol. 16, 1213–1228. https://doi.org/10.1111/j.1365-2486.2009.02094.x
5. [Banzon et al., 2016] Banzon, V., Smith, T.M., Chin, T.M., Liu, C., Hankins, W., Centers, N., 267 Ncei, I., Ave, P., 2016. *A long-term record of blended satellite and in situ sea surface tem-* 268 *perature for climate monitoring, modeling and environmental studies*. Earth Syst. Sci. Data Discuss. 0, 1–13. https://doi.org/10.5194/essd-2015-44
6. [Barth et al., 2007] Barth, J.A., Menge, B.A., Lubchenco, J., Chan, F., Bane, J.M., Kirincich, A.R., McManus, M.A., Nielsen, K.J., Pierce, S.D., Washburn, L., 2007. *Delayed upwelling* 272 *alters nearshore coastal ocean ecosystems in the northern California current*. Proc. Natl. Acad. Sci. U. S. A. 104, 3719–3724. https://doi.org/10.1073/pnas.0700462104
7. [Benazzouz et al., 2014] Benazzouz, A., Mordane, S., Orbi, A., Chagdali, M., 2014. *An improved coastal upwelling index from sea surface temperature using satellite-based approach – The case of the Canary Current upwelling system*. https://doi.org/10.1016/j.csr.2014.03.012
8. [Benoit-Bird et al., 2019] Benoit-Bird, K.J., Waluk, C.M., Ryan, J.P., 2019. *Forage Species Swarm in Response to Coastal Upwelling*. Geophys. Res. Lett. 46, 1537–1546. https://doi.org/10.1029/2018GL081603
9. [Bonino et al., 2019] Bonino, G., Masina, S., Iovino, D., Storto, A., Tsujino, H., 281 2019. *Eastern Boundary Upwelling Systems response to different atmospheric* 282 *forcing in a global eddy-permitting ocean model*. J. Mar. Syst. 197, 103178. https://doi.org/10.1016/j.jmarsys.2019.05.004

10. [Chavez and Messie´, 2009] Chavez, F.P., Messie´, M., 2009. *A comparison of* 285 *Eastern Boundary Upwelling Ecosystems*. Prog. Oceanogr. 83, 80–96. https://doi.org/10.1016/j.pocean.2009.07.032
11. Ferna´ndez-Lo´pez, J., Schliep, K., 2019. *rWind: download, edit and include* 288 *wind data in ecological and evolutionary analysis*. Ecography (Cop.). 42, 804–810. https://doi.org/10.1111/ecog.03730
12. [Largier et al., 2006] Largier, J.L., Lawrence, C.A., Roughan, M., Kaplan, D.M., Dever, E.P., Dor- 291 man, C.E., Kudela, R.M., Bollens, S.M., Wilkerson, F.P., Dugdale, R.C., Botsford, L.W., Garfield, N., Kuebel Cervantes, B., Korac˘in, D., 2006. *WEST: A northern California study of the role of wind-driven transport in the productivity of coastal plankton communities*. Deep. Res. Part II Top. Stud. Oceanogr. 53, 2833–2849. https://doi.org/10.1016/j.dsr2.2006.08.018
13. [Li et al., 2019] Li, Z., Luo, Y., Arnold, N., Tziperman, E., 2019. *Reductions in Strong Upwelling*- 296 *Favorable Wind Events in the Pliocene*. Paleoceanogr. Paleoclimatology 34, 1931–1944. https://doi.org/10.1029/2019PA003760
14. [Marrero-Betancort et al., 2020] Marrero-Betancort, N., Marcello, J., Esparrago´n, D.R., 299 Herna´ndez-Leo´n, S., 2020. *Wind variability in the Canary Current during the last 70 years*. Ocean Sci. 16, 951–963. https://doi.org/10.5194/os-16-951-2020
15. [Mendelssohn, 2018] Mendelssohn, R., 2018. *xtractomatic: accessing environmental data from ERD's ERDDAP server. R package version [WWW Document]*. URL: https://github.com/rmendels/xtractomatic
16. [Ministe`re de l'Agriculture, 2020] Ministe`re de l'Agriculture, de la P.M., Foreˆts, du D.R. et des E. et, Maritime, D. de la P., 2020. *mer en chiffre 2020*.
17. [Naulita et al., 2020] Naulita, Y., Arhatin, R.E., Nabil, 2020. *Upwelling index along the South* 307 *Coast of Java from satellite imagery of wind stress and sea surface temperature*. IOP Conf. Ser. Earth Environ. Sci. 429. https://doi.org/10.1088/1755-1315/429/1/012025
18. [Reynolds et al., 2007] Reynolds, R.W., Smith, T.M., Liu, C., Chelton, D.B., Casey, K.S., Schlax, M.G., 2007. *Daily high-resolution-blended analyses for sea surface temperature*. J. Clim. 20, 5473–5496. https://doi.org/10.1175/2007JCLI1824.1
19. [Wang et al., 2015] Wang, D., Gouhier, T.C., Menge, B.A., Ganguly, A.R., 2015. *Intensification* 313 *and spatial homogenization of coastal upwelling under climate change*. Nature 518, 390–394. https://doi.org/10.1038/nature14235
20. [Wilkerson et al., 2006] Wilkerson, F.P., Lassiter, A.M., Dugdale, R.C., Marchi, A., Hogue, V.E., 2006. *The phytoplankton bloom response to wind events and upwelled nutrients* 317 *during the CoOP WEST study*. Deep. Res. Part II Top. Stud. Oceanogr. 53, 3023–3048. https://doi.org/10.1016/j.dsr2.2006.07.007